Available online at www.sciencedirect.com
ScienceDirect
Trans. Nonferrous Met. Soc. China 34(2024) 1878−1892
Transactions of Nonferrous Metals Society of China
www.tnmsc.cn

Tailoring crystal orientation and property of Cu−Co immiscible alloy during solidification under high magnetic field

Chen WEI[1], Jin-shan LI[1], Yu-jie YAN[1], Yi-xuan HE[1], Eric BEAUGNON[2], Jun WANG[1]

1. State Key Laboratory of Solidification Processing, Northwestern Polytechnical University, Xi'an 710072, China;
2. Univ. Grenoble Alpes, INSA Toulouse, Univ. Toulouse Paul Sabatier,
EMFL, CNRS, LNCMI, 38000 Grenoble, France

Received 27 December 2022; accepted 6 August 2023

Abstract: Non-equilibrium solidification experiments were conducted on $Cu_{50}Co_{50}$ alloys under different magnetic field intensities to investigate the orientation, microstructure evolution, and magnetic properties of the Co-rich phase. The results revealed that the phase-separated rod-like Co-rich phase can realize the alignment morphology and can be oriented with the ⟨111⟩ crystal direction along the direction of the 5 T high magnetic field (HMF). In contrast, the orientation of the Cu-rich phase, which underwent secondary liquid−liquid phase separation, was not significantly affected by the HMF. The alloy solidified at 0 T showed near-magnetic isotropic behavior, while the alloy solidified at 5 T displayed magnetic anisotropic behavior. The saturation magnetization of the alloy increased slightly, and the coercivity decreased correspondingly, which were strictly dependent on the orientation evolution of the Co-rich crystal.
Key words: high magnetic field; microstructure evolution; Cu−Co alloy; phase separation; magnetic property

1 Introduction

In recent decades, a long-standing interest has focused on metastable immiscible alloys due to their unique microstructure and potential to exhibit exceptional physical properties [1]. For immiscible alloys, most previous studies have focused mainly on the adjustment of typical core-shell microstructures with liquid−liquid phase separation by altering the volume fraction of two phases, undercooling and nucleation during the solidification process [2−4]. However, the experimental results have not been satisfactory, as it is difficult to actively control the microstructure. Consequently, it is necessary to note that the final solidified orientation and texture are critical for both the growth behavior of the crystal and magnetic property of the alloy [5,6]. Several studies have shown that applying alignment or preferred orientation can enhance the physical properties of materials [7].

By adjusting the microstructure and promising properties such as the giant magnetoresistance effect, an alternative method was proposed to control the orientation of the crystal during the solidification process under extreme conditions, which has been recognized as a valid approach to improve the properties of materials. The application of high magnetic field (HMF) is a promising technology and has been shown to create novel functions and phenomena, particularly in materials processing [8,9]. A significant amount of research has concentrated on the experimental and theoretical analyses of grain alignment structures and crystal orientation utilizing the solidification process [10] with the aid of the HMF.

Corresponding author: Jun WANG, Tel: +86-29-88460294, E-mail: nwpuwj@nwpu.edu.cn;
Jin-shan LI, Tel: +86-29-88460568, E-mail: ljsh@nwpu.edu.cn
DOI: 10.1016/S1003-6326(24)66513-1

It has become an intriguing method due to the remarkable influence of HMF on the crystal orientation [11,12], solute redistribution [13] and melt flows [14,15]. Especially in the solidification process, the crystalline material could be driven to rotate with freedom by the external magnetic field to reduce the system energy [16]. It has been found that these magnetic field effects are not limited to ferromagnetic materials, but also extend to non-magnetic materials [17]. For instance, LIU et al [18] reported that the Fe−1.0wt.%Si alloy prepared via a magnetic field during solidification exhibits excellent magnetic property, which was attributed to the change in crystal orientation induced by the magnetic field. Similarly, LIU et al [19] found that as the magnetic field intensity increased, the crystal orientation of the Fe−6.5Si−0.05B alloy evolved and thus led to a change in magnetic property. DONG et al [20] also observed a rotation of the primary $(Tb,Dy)Fe_3$ phase and its effect on the orientation change of the peritectic $(Tb,Dy)Fe_2$ phase in response to a high magnetic field. Additionally, RANGO et al [6] experimentally demonstrated that high magnetic fields can still induce magnetic orientation of ferromagnetic materials at high temperature, and oriented $YBa_2Cu_3O_7$ materials were prepared at high temperature by solidification under a magnetic field of 5 T. Despite attempts to investigate the formation mechanism of the grain orientation structure [21], it is still obscure owing to the complexity of the mechanism and diversity of phenomena for different alloys.

The Cu−Co alloy is a relatively simple binary immiscible alloy system with a well-known giant magnetoresistance effect [22], which normally exhibits a wide metastable immiscible region and experiences liquid−liquid phase separation during the cooling process [23]. The key problem that restricts the industrial application of immiscible alloys with liquid−liquid phase separation lies in the control of their microstructure. After the phase separation, the Cu−Co alloy forms a Co-rich phase at room temperature, which exhibits a stronger magnetism at high temperatures under HMF compared to the diamagnetic Cu-rich phase. The strong paramagnetism of the Co-rich phase makes it more susceptible to HMF. Therefore, it is feasible to realize effective control of one of the phases in immiscible alloys based on HMF technology. Previous studies have analyzed the microstructure evolution of Cu−Co alloys based on various magnetic field effects [24,25]. In previous study [26], we demonstrated that applying a high magnetic field during the solidification of a $Cu_{66.67}Co_{33.33}$ alloy can significantly affect the liquid−liquid phase separation behavior of the Cu−Co immiscible alloy. The results showed that the elongation of Co-rich phase along the magnetic field direction is due to the static magnetic energy.

However, the previous analysis was based on theoretical calculations, and the relationship between microstructure evolution and crystal structure is usually easy to neglect. Therefore, in this study, we aim to explore the influence of HMF on the crystal structure of immiscible alloys during non-equilibrium solidification from the perspective of crystal orientation and crystal growth. Our method enables tailoring the crystal orientation, microstructure evolution, and magnetic properties of immiscible alloys during the non-equilibrium solidification process without pre-processing.

2 Experimental

The method of glass fluxing combined with the cyclic overheating technique was adopted to realize the undercooling experiment. A master alloy of Cu−50at.%Co was prepared using arc-melting with a mixture of high-purity copper (99.99 wt.%) and cobalt (99.99 wt.%) in a high-purity argon atmosphere. The master ingots were then cut into a few cuboid candidate specimens (with an average mass of about 1 g) for the undercooling experiments under different magnetic field intensities. The sample was placed in a quartz glass tube and then inserted into the maximum heating area of the SiC high-temperature resistance heating furnace, that is, the center area of the HMF device. A detailed description of this device is shown in Ref. [27]. The samples were repeatedly superheated, melted and solidified to achieve the desired undercooling. Finally, the samples were quenched at 1000 °C.

After the solidification experiment under 0 T, and 5 T magnetic fields, the magnetic field-treated samples were cut and polished along the direction parallel (longitudinally) and perpendicular (transversely) to the magnetic field to characterize the morphologies by micro-CT (nanoVoxel 3000),

optical microscopy (OM, GX71) and scanning electron microscopy (SEM, Helios G4 CX) with etching. The inverse pole figure (IPF) orientation analysis of the specimens in the microstructure was examined by electron backscatter diffraction (EBSD) mapping on SEM (FEI Quanta 650F) and with HKL channel 5 data acquisition and analysis. The chemical compositions of the phases in the specimens were analyzed via energy dispersive X-ray spectrometry (EDX) on EBSD. Crystal structures of phase constituents were identified by X-ray diffraction (XRD, D8 ADVANCE). The hysteresis loops of various samples were detected by Cryogenic CFMS-14T physical property measurement system (PPMS) at 298 K within the field range of $\pm 1.5916\times10^6$ A/m.

3 Results and discussion

3.1 Microstructure evolution of Cu−Co alloy under various magnetic fields

The phase constitution of the sample solidified with an undercooling of 209 K under 0 T was investigated via X-ray diffraction with a circumrotating Cu target, as shown in Fig. 1. The diffraction peaks were indexed to two face-centered cubic solid solutions. A set of stronger peaks correspond to the Cu-rich solid solution, while a set of weaker peaks correspond to the Co-rich solid solution in the $Cu_{50}Co_{50}$ immiscible alloy.

Figure 2(a) shows the characteristic microstructure of the $Cu_{50}Co_{50}$ alloy solidified under 0 T magnetic field with an undercooling of 209 K,

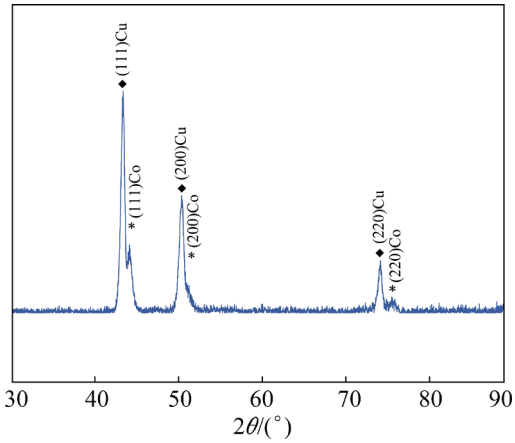

Fig. 1 XRD pattern of $Cu_{50}Co_{50}$ alloy with undercooling of 209 K under 0 T

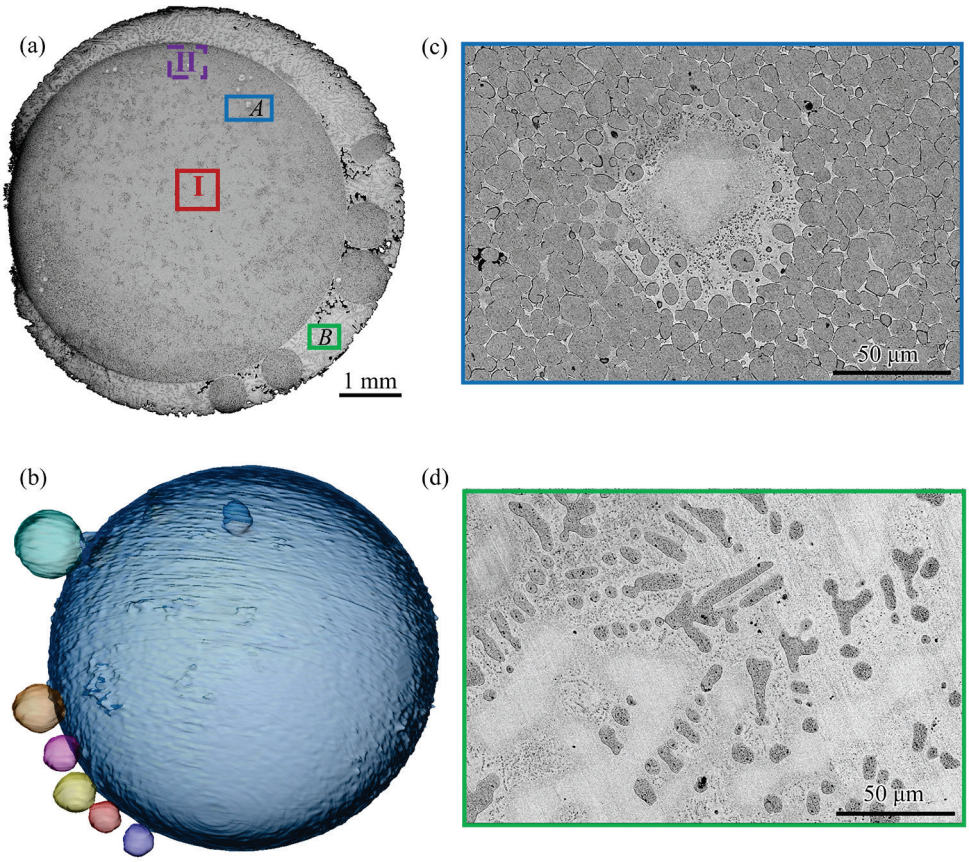

Fig. 2 Microstructure of $Cu_{50}Co_{50}$ alloy solidified under 0 T magnetic field with undercooling of 209 K: (a) Overview OM image; (b) 3-dimensional microstructure of (a); (c, d) SE images of Regions *A* and *B* in (a), respectively

which indicates the occurrence of liquid−liquid phase separation, i.e., the core-shell structure [28]. Due to the limitation of the two-dimensional section on the observation of the internal morphology of the alloy, the 3-dimensional microstructure is depicted in Fig. 2(b), which presents the distribution of the spherical Co-rich phase in the integral sample. It should be noted that the coarsening process of the spherical Co-rich phase occurs in order to decrease the energy of the whole system. Figure 2(c) shows a partially enlarged view of the phase-separated Co-rich phase in Fig. 2(a), where it can be seen that the Co-rich phase consists of approximately equiaxed grains. As explained elsewhere [28], the white spherical region corresponds to the Cu-rich phase, which has experienced secondary liquid−liquid phase separation and has been generated within the phase-separated Co-rich phase. The Co-rich phase mainly consists of the Fcc-Co phase, which results from liquid−liquid phase separation. A large number of α-Co dendrites and nano-sized Co-rich precipitates are found to be distributed in the Cu-rich matrix as shown in Fig. 1(d), which is consistent with our previous research results [28].

The transverse microstructure of the $Cu_{50}Co_{50}$ alloy solidified under 5 T magnetic field with an undercooling of 219 K is exhibited in Fig. 3(a). It can be observed that the morphology of the phase-separated Co-rich phase has changed obviously and no longer appears regular spherical. At the edge region of the sample, the Co-rich phase is evidently deformed, while in the central region of the sample, the size of the Co-rich phase decreases and the annular structure is observed in the center. The 3-dimensional microstructure in Fig. 3(b) shows that the Co-rich phases occupy different regions of the alloy with varying colors. Figure 3(c) presents a locally enlarged view displaying that the Co-rich phase is still composed of grains with different sizes and that a significant secondary liquid−liquid phase separation phenomenon has occurred. Meanwhile, Fig. 3(d) displays a large number of α-Co dendrites and nano-sized Co-rich precipitates in the Cu-rich matrix.

The longitudinal microstructure of the $Cu_{50}Co_{50}$ alloy solidified under 5 T magnetic field with an undercooling of 219 K is shown in Fig. 4(a). The imposition of the magnetic field is found to have a notable influence on the morphology of the Co-rich phase on account of the metastable liquid−liquid phase separation. The Co-rich phase with a rod-like shape appears to be elongated along the direction of the magnetic field. In addition, Fig. 4(b) displays

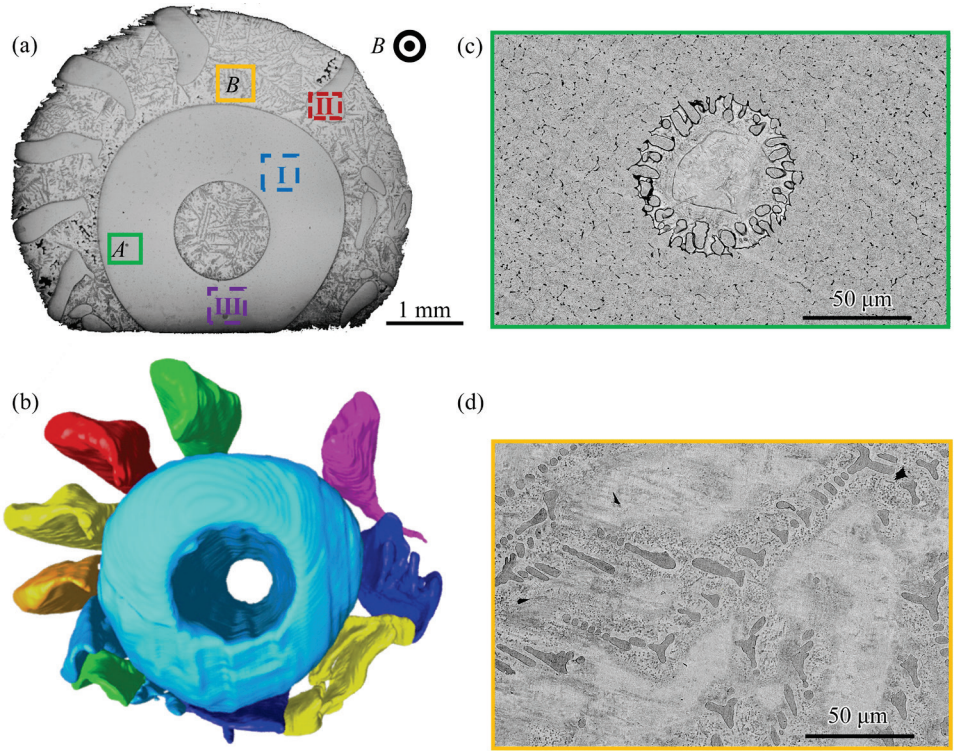

Fig. 3 Transverse microstructure of $Cu_{50}Co_{50}$ alloy solidified under 5 T magnetic field with undercooling of 219 K: (a) Overview OM image; (b) 3-dimensional microstructure of (a); (c, d) SE images of Regions *A* and *B* in (a), respectively

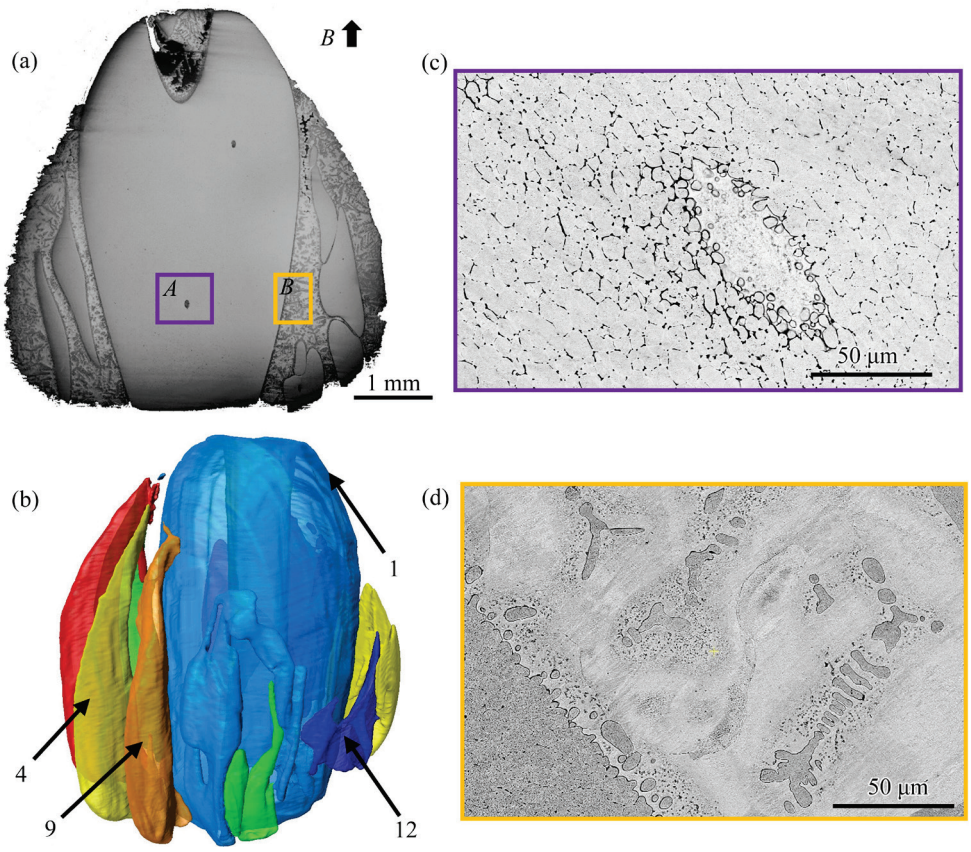

Fig. 4 Longitudinal microstructure of $Cu_{50}Co_{50}$ alloy solidified under 5 T magnetic field with undercooling of 219 K: (a) Overview OM image; (b) 3-dimensional microstructure of (a); (c, d) SE images of Regions *A* and *B* in (a), respectively (The numbers of rod-like Co-rich phases with different sizes are indicated by corresponding black arrows)

the 3-dimensional microstructure of Fig. 4(a), featuring rod-like Co-rich phases with different length to diameter ratios distributed throughout the whole sample. In addition, videos of the 3-dimensional microstructure of the alloys with liquid phase separation can be found in the supplementary file. Figure 4(c) shows an enlarged view of the box area in Fig. 4(a), exhibiting that the Cu-rich phase with a secondary liquid−liquid phase separation occurs within the Co-rich phase, which is also in the form of a rod-like shape. The phase-separated interface between the rod-like Co-rich phase and the Cu-rich matrix phase is illustrated in Fig. 4(d). It can be observed that the fragmented Co-rich dendrites and nano-sized Co-rich precipitates are dispersed in the Cu-rich matrix.

3.2 Orientation characteristics of solidified microstructure under different magnetic fields

The results of this work are similar to those of our previous studies [28], but with some differences, it is noted that in the absence of a magnetic field, the solidified $Cu_{66.67}Co_{33.33}$ and $Cu_{50}Co_{50}$ alloys both exhibit a core-shell structure due to convection and a temperature gradient. The Co-rich phases in Cu−Co alloys with different compositions are elongated parallel to the magnetic field, which is attributed to the magnetization energy. The distribution of the Co-rich phase in $Cu_{66.67}Co_{33.33}$ alloys is relatively uniform perpendicular to the magnetic field after the application of a high magnetic field. Based on theoretical analysis and calculation, we have discussed the morphological evolution mechanism of the Co-rich phase in the $Cu_{66.67}Co_{33.33}$ alloy under a 10 T magnetic field, and further detailed characterization is still lacking. In contrast, under a 5 T magnetic field, the Co-rich phase in the $Cu_{50}Co_{50}$ alloy in this paper is only uniformly distributed in the edge region perpendicular to the magnetic field direction, and the middle region presents the annular microstructure. To further analyze the different distribution morphologies of these two Co-rich regions in $Cu_{50}Co_{50}$ from the perspective of crystal

structure, the orientation characteristics of the solidified microstructure were analyzed via EBSD technology. Figure 5 displays the EBSD analysis of Region I in Fig. 2(a). Figure 5(a) presents the IPF orientation map for the spherical Co-rich phase in the $Cu_{50}Co_{50}$ alloy. It is worth noting that the grains in different regions of the Co-rich phase possess various colors revealing that the crystals have different orientations. The distribution histogram of grain size is quantified and exhibited in Fig. 5(b). The grain size distribution of the Co-rich phase is symmetrical, and the area fraction of grains with a size of 7 μm is approximately 19%. Figure 5(c) shows the corresponding pole figure of the Co-rich phase in Fig. 5(a). This indicates that the {110}⟨001⟩ Goss texture appears in the sample.

Figure 6 shows the EBSD analysis corresponding to Area I in Fig. 3(a). Figure 6(a) presents the IPF orientation map for the annular Co-rich phase in the $Cu_{50}Co_{50}$ alloy under 5 T magnetic field. It can be seen that the orientation distribution of the Co-rich phase solidified under 5 T magnetic field is relatively uniform. The distribution histogram of grain size is quantified and illustrated in Fig. 6(b). The grain size distribution of the Co-rich phase is more asymmetrical and larger grains appear in the central region of the Co-rich phase compared with that of the alloy treated without a magnetic field. This can be attributed to the fact that grains with the same orientation coalesce and grow [29]. Figure 6(c) presents the corresponding pole figure of the Co-rich phase in Fig. 6(a). It is found that the {100}⟨001⟩ cube texture emerges in the sample. The above-described results manifest that when the HMF is imposed, the orientation relationship of the Co-rich phase in the $Cu_{50}Co_{50}$ alloy can be influenced. The corresponding inverse pole figure map of the Co-rich phase is displayed in Fig. 6(d), and it can be found that a relatively weak ⟨001⟩ orientation parallel to the X_0-axis in the sample is generated.

Compared to the morphology of the Co-rich phase observed in the $Cu_{50}Co_{50}$ alloy without the magnetic field, the microstructure of the Co-rich phase at the edge of the sample is obviously altered under 5 T magnetic field. Figure 7 shows the EBSD analysis corresponding to Region II in Fig. 3(a). Figure 7(a) presents the IPF orientation map for the Co-rich phase at the edge of the alloy. It can be found that the crystal orientation of the Co-rich phase solidified at 5 T magnetic field is random. The distribution histogram of grain size is quantified and presented in Fig. 7(b). The grain size distribution of the Co-rich phase is inhomogeneous and a small number of large grains appear compared with that

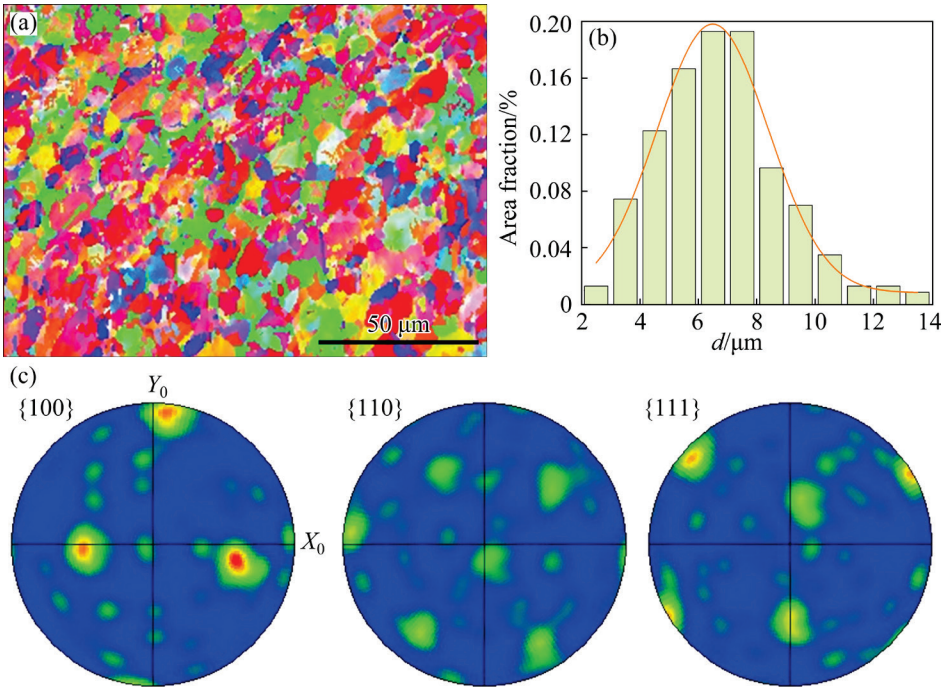

Fig. 5 EBSD analysis of microstructure shown in red box in Fig. 2(a): (a) IPF orientation map for Co-rich phase; (b) Grain size distribution of Co-rich phase; (c) Corresponding pole figure maps

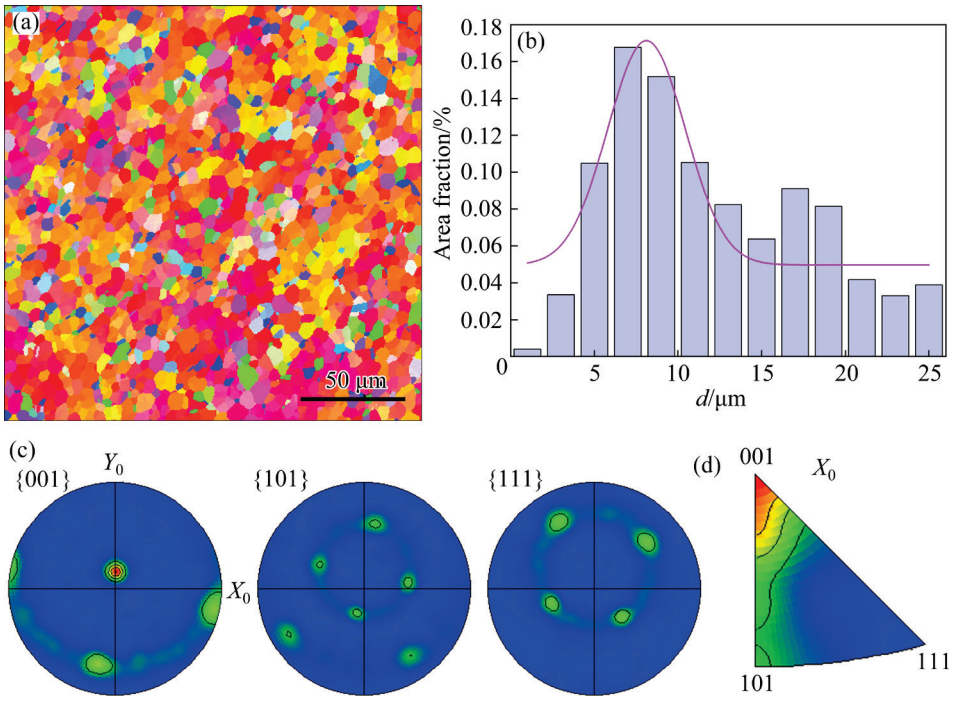

Fig. 6 EBSD analysis of microstructure of dotted boxed Region I in Fig. 3(a): (a) IPF orientation map for Co-rich phase; (b) Grain size distribution of Co-rich phase; (c) Corresponding pole figure maps; (d) Corresponding inverse pole figure map

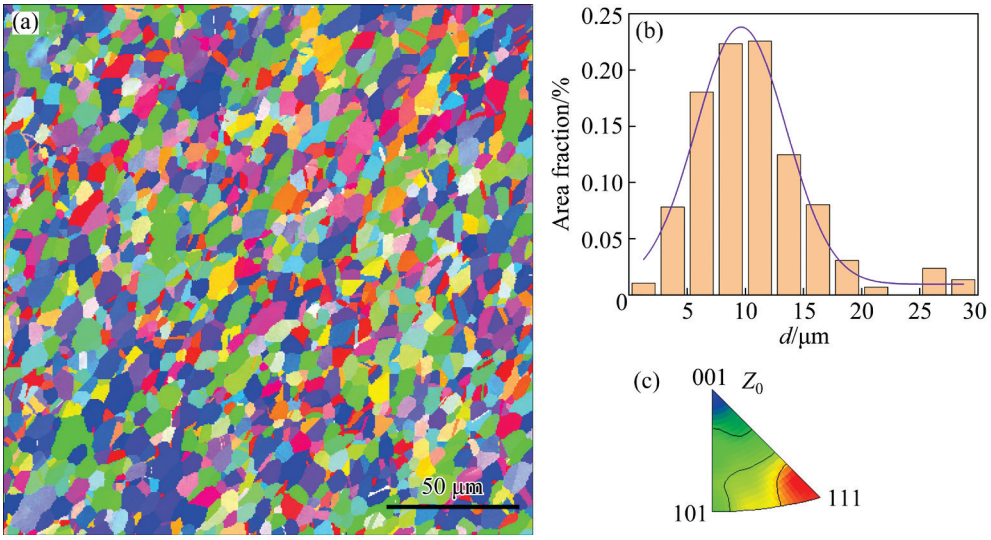

Fig. 7 EBSD analysis of microstructure of Region II in Fig. 3(a): (a) IPF orientation map for Co-rich phase; (b) Grain size distribution of Co-rich phase; (c) Corresponding inverse pole figure map

of the alloy treated without a magnetic field. Figure 7(c) shows the corresponding inverse pole figure map of the Co-rich phase in Fig. 7(a). It should be noted that a relatively weak ⟨111⟩ orientation parallel to the Z_0-axis in the sample is formed. However, the Z_0-axis is in the direction applied by the HMF, that is, the Co-rich phase at the edge of the sample forms an orientation that is parallel to the magnetic field.

Figure 8 exhibits EBSD analysis of the Cu-rich phase that experienced secondary liquid−liquid phase separation in the $Cu_{50}Co_{50}$ alloy under 0 T and 5 T magnetic fields. Figure 8(a) presents the IPF orientation map for the Cu-rich phase with secondary liquid−liquid phase separation corresponding to Region II in Fig. 2(a). The orientation distribution of the Cu-rich phase is relatively concentrated. The EDS mappings shown in Figs. 8(a_1) and (a_2)

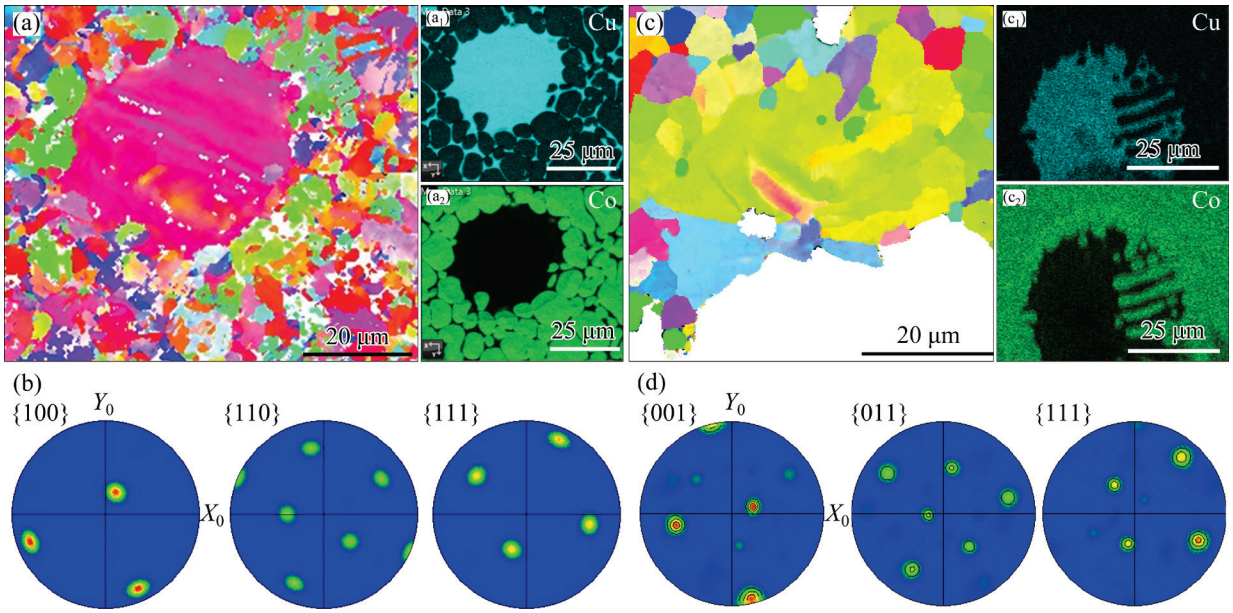

Fig. 8 (a) EBSD analysis of microstructure of Region II in Fig. 2(a); (a_1, a_2) EDS maps of position in (a) and corresponding elements Cu and Co, respectively; (b) Corresponding pole figure map in Fig. 8(a); (c) EBSD analysis of microstructure of Region III in Fig. 3(a); (c_1, c_2) EDS maps of position in (c) and corresponding elements Cu and Co, respectively; (d) Corresponding pole figure map in Fig. 8(c)

illustrate the distribution of the elements, indicating that the copper element is mainly abundant in the Cu-rich phase area. Figure 8(b) presents the corresponding pole figure map for the Cu-rich phase in Fig. 8(a), which is similar to that of the Co-rich phase under 0 T magnetic field, as shown in Fig. 5(c). Figure 8(c) shows the IPF orientation map for the Cu-rich phase with secondary liquid−liquid phase separation corresponding to Region III in Fig. 3(a). With the application of 5 T magnetic field, the orientation of the Cu-rich phase is almost the same. The EDS mappings displayed in Figs. 8(c_1) and (c_2) present the distribution of the elements, indicating that secondary liquid−liquid phase separation occurred. Moreover, as shown in Fig. 8(d), the corresponding pole figure map shows the same texture component as in the alloy without a treated magnetic field. It can be inferred that the orientation and texture component of the Cu-rich phase with secondary liquid−liquid phase separation are not appreciably affected by the application of HMF.

3.3 Influence of microstructural change on magnetic properties of alloys

The microstructure results indicated that the orientation behavior of the crystal is closely associated with the magnetic field, and therefore, the HMF has an influence on the magnetic properties of the alloys accordingly. The hysteresis loops of $Cu_{50}Co_{50}$ alloys were tested at room temperature with various magnetic fields and are displayed in Fig. 9(a). The results clearly reveal that the alloy solidified in a magnetic field of 0 T exhibits near-magnetic isotropic behavior due to the overlap of the hysteresis loops in two different directions, as displayed in Fig. 9(a_1), while the alloy solidified in a magnetic field of 5 T presents pronounced magnetic anisotropic behavior, as shown in Fig. 9(a_2). For the alloy with an undercooling of 209 K in the absence of a magnetic field, the value of the saturation magnetization (M_s) is 60.62 A·m^2/kg and the coercivity is 8427.522 A/m. In contrast, the value of the saturation magnetization is 65.73 A·m^2/kg, and the coercivity is 6602.753 A/m in the alloy with an undercooling of 219 K under 5 T magnetic field. It should be emphasized that the application of HMF results in a slight increase in saturation magnetization and corresponding decrease in coercivity. It is speculated that the variation in magnetic properties with magnetic field intensity can be linked to the orientation evolution of the Co-rich crystal. Meanwhile, it can be observed that

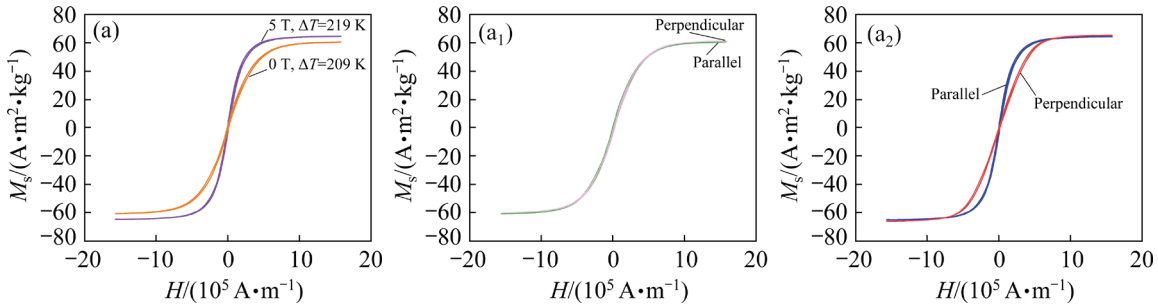

Fig. 9 (a) Magnetic hysteresis loops at room temperature of $Cu_{50}Co_{50}$ alloys in parallel magnetic field direction: (a_1) Magnetic hysteresis loops of alloy at 209 K under 0 T; (a_2) Magnetic hysteresis loops of alloy at 219 K under 5 T (H: Applied magnetic field intensity)

the saturation magnetization of the alloy tested parallel to the imposed magnetic field is easier than that tested perpendicular to the imposed magnetic field, which accounts for the alignment of Co-rich crystals and the formation of the ⟨111⟩ orientation in the direction parallel to the magnetic field. The alignment of the Co-rich phase is oriented, which reduces the obstruction of magnetic domain rotation along a certain direction [19], and results in a significant decrease in coercivity. Moreover, grain boundaries can hinder the movement of magnetic domain walls [5]. The coercivity of the alloy treated with an HMF is lower than that of the alloy without magnetic field, which is also related to the number of large grains increasing and the grain boundary density decreasing, as shown in Figs. 6 and 7.

The saturation magnetization is an intrinsic property of matter, depending on the composition and other intrinsic parameters. When a 5 T magnetic field is applied, the Co-rich phase in the microstructure preferentially follows the preferential ⟨111⟩ direction, which is parallel to the applied magnetic field. As a result, the magnetized atoms are especially easily oriented along the direction parallel to the imposed magnetic field. The increase in alignment in the phases of $Cu_{50}Co_{50}$ alloys under the action of a magnetic field may give rise to the strengthening of the total dipoles of the atom, thus enhancing its saturation magnetization [30]. Additionally, the chemical composition (at.%) of cobalt in different phases of $Cu_{50}Co_{50}$ alloys measured by EDS is shown in Table 1. It can be clearly observed that the cobalt solute content in the Co-rich phase and Co-rich dendrites increases obviously, while the cobalt solute content in the Cu-rich matrix phase decreases after the application of 5 T magnetic field. Due to the fact that the Co content in the Cu-rich phase may be different at different locations, an EDS line scan perpendicular to the Co phase boundary in the $Cu_{50}Co_{50}$ alloy without and with a magnetic field is presented in Fig. 10. It is evident that the solute content of the Co-rich phase in the Cu-rich matrix decreases significantly with the application of a magnetic field. Therefore, the increase in saturation magnetization of the alloy can be attributed to the increase in the contribution of the cobalt solute content in the Co-rich phase.

3.4 Microstructure evolution mechanism of alloys under high magnetic field

Under certain conditions, owing to the shape of the crystal, shape magnetic anisotropy can also result in magnetic alignment, such as the needle-like phase separated from a liquid metal [16,31]. Based on the anisotropy of magnetocrystalline [32], the orientation of the particles may be altered due to the application of the HMF. It is well known that the HMF is able to influence the energy of a solidified alloy system, as it can transfer non-contact magnetic energy to the material. The crystal orientation induced via a magnetic field has been extensively researched, and a model of the rotation orientation mechanism has been proposed [33]. Three aspects must be satisfied for a crystal with an aligned structure and orientation by applying a magnetic field.

The first condition is that the unit crystal cells of the materials should have magnetic anisotropy. In general, materials with magnetic anisotropy have different magnetic susceptibilities in each crystal direction, which allows them to align with a

Table 1 Chemical composition of cobalt in different phases of $Cu_{50}Co_{50}$ alloys under different magnetic field intensities and undercoolings

B/T	Δ*T*/K	Content/at.%		
		Co-rich phase	Cu-rich phase	*α*-Co dendrite
0	209	81.88±0.5	5.53±0.7	78.81±0.3
5	219	84.46±0.3	4.82±0.5	79.26±0.4

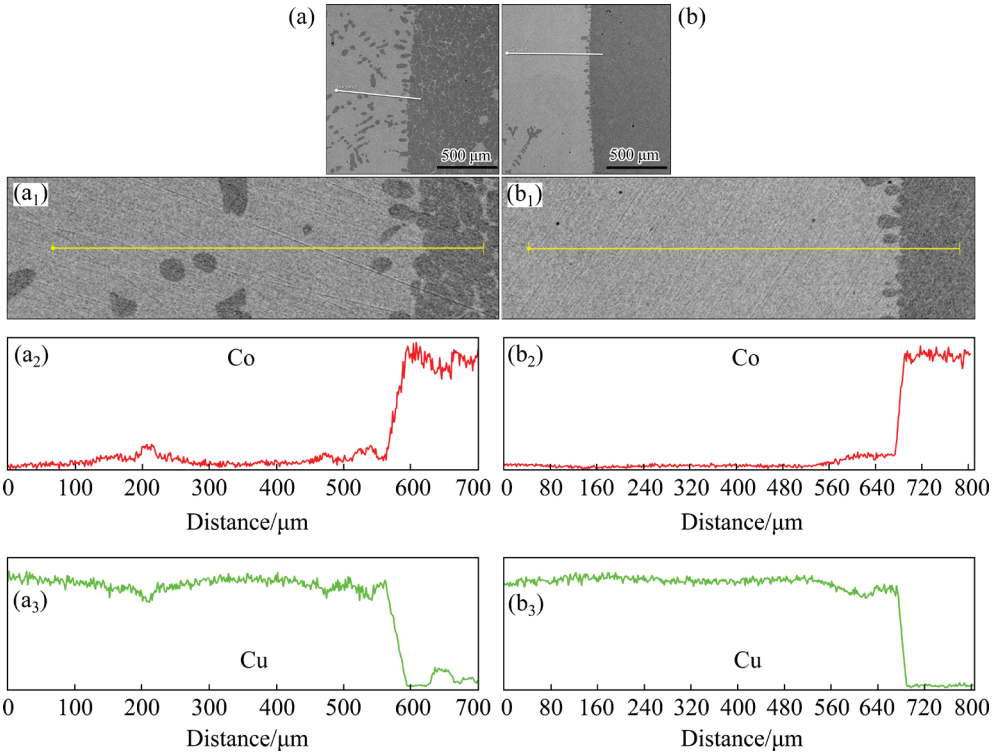

Fig. 10 (a) EDS line scan perpendicular to Co phase boundary without magnetic field in $Cu_{50}Co_{50}$ sample; (b) EDS line scan perpendicular to Co phase boundary with high magnetic field in $Cu_{50}Co_{50}$ sample; (a_1, b_1) Location and length of line corresponding (a, b), respectively; (a_2, a_3, b_2, b_3) Elemental concentrations along line (a_1, b_1), respectively

preferred direction. Additionally, it is worth noting that the hysteresis loops in Fig. 9(a_2) show significant indications of magnetic anisotropy. Previous studies have shown that a temperature range exists beneath the liquidus line within which an aligned crystal structure can be obtained by applying an external magnetic field [34]. Combined with the above microstructural analysis, it can be concluded that HMF has a certain influence on the alignment of crystals, which can be explained via the following theory. On the basis of the magnetic properties of the crystal and the melt, the magnetic field oriented the crystallized nucleus of the melt in a definite direction. The mechanical force moment leading to the alignment of the crystal in the melt mainly depends on the magnetic properties of the nucleus as well as the degree of uniformity of the HMF [34]. It is worth noting that anisotropic crystals are also subject to the torque caused by the demagnetizing field, but this torque is usually much smaller than that caused by magnetic anisotropy with the exception of very magnetic systems [35]. Consequently, the magnetic torque is one of the main reasons for the change in the crystal alignment. As the particle is precipitated from the melt, the magnetization (M) is produced owing to the applied magnetic field, and the magnetic torque T acting on the crystal with magnetic anisotropy in the homogeneous magnetic field can be written as [36]

$$T = \frac{\Delta\chi}{2\mu_0} B^2 V \sin 2\alpha \tag{1}$$

where $\Delta\chi$ is the magnetic susceptibility difference between the two mutually-perpendicular axes of the crystal, B is the magnetic field intensity, μ_0 is the magnetic permeability constant in vacuum, V is the

volume of crystal, and α is the angle between the axis with maximum magnetic susceptibility and B. If the crystal with magnetic anisotropy is put in HMF, the crystal will rotate freely [37]. Therefore, the specimen solidified at 5 T shows an alignment structure that is parallel to the magnetic field direction.

The second case is that the material exists in a weakly constrained medium that can rotate sufficiently [33]. In other words, the surrounding melt can offer a weak constraint medium that ensures the free rotations of the crystal, indicating that in this case, the material will be surrounded by a fluid. Once the rotation begins, the resistance caused by the liquid viscosity and the Lorentz force will hinder the rotation, and therefore the magnetic field will be high enough for the magnetic torque to overcome the resistance. Another crucial factor that influences the rotation of the crystal is time. In the experiment, the supersaturated Co-rich phase separated from the Cu-rich melt at an undercooling of 219 K, and the time was long enough for the Co-rich phase to be rotated by the magnetic torque prior to the liquid Cu-rich phase solidifying completely under the magnetic field.

The third condition is that the magnetization energy is greater than the thermal disorder energy. The Cu−Co alloy has apparent magnetocrystalline anisotropy and the value of its magnetization energy is larger than the thermal disorder energy, in which it has enough rotation time and space to make the crystal rotate and align under the HMF. The magnetic field causes the orientation of the crystal by rotating the magnetized crystal to reach a stable orientation, thereby reducing the magnetization energy. If the non-ferromagnetic material is magnetized in a magnetic field, the magnetization energy of the material can be written as [38]

$$U=-\int_0^{H_{ex}}\mu_0 M\mathrm{d}H_{eff} \tag{2}$$

where H_{ex} is the magnetic field applied outside of the material, and H_{eff} is defined by considering the demagnetization field, which is the magnetic field generated inside the material. The relation between $M=\chi H_{eff}$ and $H_{eff}=H_{ex}-NM$ is as follows [39]:

$$H_{ex}=(1+N\chi)H_{eff} \tag{3}$$

The magnetization energy in crystal orientations can be expressed as [38]

$$U=-\frac{\mu_0\chi}{2\left(1+N\chi\right)^2}H_{ex}^2 \tag{4}$$

where N is the demagnetization factor, and χ is the magnetic susceptibility.

The demagnetizing field H_d is also uniform in any homogeneous magnetized sample with the ellipsoid form. The demagnetizing factor for an ellipsoid of revolution with $\alpha=c/a>1$ can be calculated as [40]

$$N=\frac{1}{\left(\alpha^2-1\right)}\left[\frac{\alpha}{\sqrt{\alpha^2-1}}\cosh^{-1}(\alpha)-1\right] \tag{5}$$

$$\alpha=c/a \tag{6}$$

where c is the length of long axis of rotation of the ellipsoid, and a is the transverse diameter.

To further understand the magnetic alignment of the Co-rich phase in the Cu−Co alloy, the demagnetizing factors were calculated for different length-diameter ratios, as shown in Table 2. Based on Eq. (5), the calculated demagnetizing factors were plotted as a function of length-diameter ratio in Fig. 11. The demagnetizing factors decrease as

Table 2 Length−diameter ratio (c/a) of Co-rich phase in $Cu_{50}Co_{50}$ alloy with parallel 5 T magnetic field at 219 K undercooling (number represents rod-like Co-rich phase with different sizes, and their values counted by 3-dimensional CT, as shown in Fig. 4)

Number	c/a
1	1.96
2	3.89
3	4.3
4	3.8
5	4.05
6	3.3
7	3.06
8	3.14
9	3.68
10	3.43
11	2.66
12	4.79
13	2.61
14	4.35
15	4.66

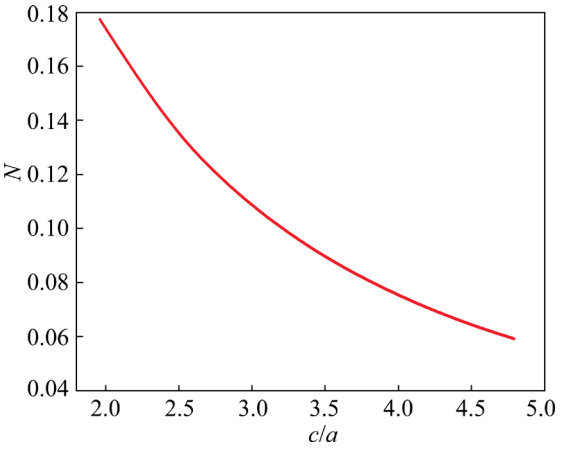

Fig. 11 Calculated demagnetizing factors as function of Co-rich phase length−diameter ratio under 5 T magnetic field with 219 K undercooling

the length-diameter ratio of the Co-rich phase increases. Based on the points discussed above, when the crystal is placed in a magnetic field, the crystal prefers to be arranged in the favorable direction to minimize the magnetization energy, thus stabilizing the system. Combining Fig. 11 and Eq. (4), it can be inferred that the Co-rich phase at the edge of the alloy has a higher magnetization energy due to a larger length-diameter ratio under 5 T magnetic field, while the Co-rich phase with the smallest length-diameter ratio in the center of the alloy has the minimum magnetization energy. Based on the above mechanism, when the Co-rich phase having the magnetic anisotropy is dispersed in a liquid matrix and subjected to a magnetic field, the Co-rich phase with higher magnetization energy will be rotated at an angle to decrease the system energy, forming the oriented structure.

Previous studies have shown that the magnetic field during solidification can cause an aligned microstructure through the free rotation of the crystals with the magnetic anisotropy, which indicates that the aligned microstructure comes from the improvement of the crystal ordering degree [30]. To gain a better understanding of the evolution of the crystal alignment and orientation during non-equilibrium solidification, a schematic illustration of the evolution of the Co-rich crystal is illustrated in Fig. 12 under different magnetic field intensities. It can be observed that the Co-rich crystals are oriented arbitrarily within the core Co-rich phase in the absence of a magnetic field. However, with the application of an HMF, the phase separated Co-rich phase exhibits an aligned morphology, forming a rod-like structure. When the length-diameter ratio of the rod-like Co-rich phase is large, the Co-rich crystal is oriented along the ⟨111⟩ direction induced by the HMF during the non-equilibrium solidification process. This demonstrates that the HMF can effectively tailor the orientation of the crystal and alignment of the separated phase in immiscible alloy during non-equilibrium solidification.

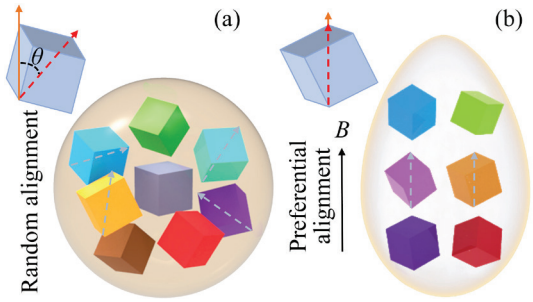

Fig. 12 Schematic illustration of evolution of Co-rich crystal: (a) Random orientation within core Co-rich phase in the absence of magnetic field; (b) Preferential alignment and orientation within rod-like Co-rich phase when HMF is imposed

4 Conclusions

(1) The phase-separated Co-rich phase solidified at 0 T has no pronounced alignment and orientation behavior. In contrast, the Cu-rich phase in the alloy exhibits the same orientation feature, irrespective of whether the HMF is imposed. Therefore, the magnetic field has no obvious influence on the orientation of the Cu-rich phase with secondary liquid−liquid phase separation.

(2) The application of a 5 T magnetic field causes the phase-separated Co-rich phase to exhibit aligned morphology due to magnetic torque. The Co-rich phase at the edge of the sample is oriented along ⟨111⟩ crystal direction parallel to the magnetic field, which is attributed to larger length-diameter ratios of crystals aligning in the direction to minimize magnetization energy.

(3) The sample solidified at 0 T presents near-magnetic isotropic behavior, whereas the sample solidified at 5 T displays magnetic anisotropy. With the application of HMF, the saturation magnetization of the alloy increases slightly due to enhanced total dipoles of the atom

and increased contribution of cobalt solute content within the Co-rich phase, while the decrease in coercivity is attributed to the reduction of the obstruction of magnetic domain rotation.

CRediT authorship contribution statement

Chen WEI: Investigation, Writing − Original draft, Visualization, Formal analysis; **Jin-shan LI:** Supervision, Funding acquisition; **Yu-Jie YAN** and **Yi-xuan HE:** Investigation, Data curation; **Eric BEAUGNON:** Investigation, Methodology; **Jun WANG:** Data curation, Writing − Review & editing.

Declaration of competing interest

The authors declare no conflict of interest. The funders had no role in the design of the study; in the collection, analyses, or interpretation of data; in the writing of the manuscript, or in the decision to publish the results.

Data availability

All data are available from the corresponding author on reasonable request.

Acknowledgments

This work was supported by the National Natural Science Foundation of China (Nos. 51690163, 52174375), the Fund of the State Key Laboratory of Solidification Processing in NWPU, China (No. 2021-TS-01), the Innovation Capability Support Program of Shaanxi Province, China (No. 2020KJXX-073), and the Fundamental Research Funds for the Central Universities, China.

References

[1] CHEN Lian-yi, XU Jia-quan, HONGSEOK C, HIROMI K, JIN Song, LI Xiao-chun. Rapid control of phase growth by nanoparticles [J]. Nature Communications, 2014, 5: 3879.

[2] YANG Wei, CHEN Shou-hui, YU Huan, LI Sheng, LIU Feng, YANG Gen-cang. Effects of liquid separation on the microstructure formation and hardness behavior of undercooled Cu−Co alloy [J]. Applied Physics A, 2012, 109(3): 665−671.

[3] ZHAO Dan-dan, YANG Fan, HOLLAND-MORITZ D, KOLBE M, BUSLAPS T, GAO Jian-rong. In situ studies of liquid-liquid phase separation, solidification sequence and dendrite growth kinetics in electrostatically levitated Ti−Y alloys [J]. Acta Materialia, 2021, 213: 116962.

[4] WANG Meng, YANG Qian-ru, JIANG Yan-bin, LI Zhou, XIAO Zhu, GONG Shen, WANG Yong-ru, GUO Chuang-li, WEI Hai-gen. Effects of Fe content on microstructure and properties of Cu−Fe alloy [J]. Transactions of Nonferrous Metals Society of China, 2021, 31(10): 3039−3049.

[5] FU Hua-dong, ZHANG Zhi-hao, JIANG Yan-bin, XIE Jian-xin. Improvement of magnetic properties of an Fe−6.5wt.%Si alloy by directional solidification [J]. Materials Letters, 2011, 65(9): 1416−1419.

[6] de RANGO P, LEES M, LEJAY P, SULPICE A, TOURNIER R, INGOLD M, GERMI P, PERNET M. Texturing of magnetic materials at high temperature by solidification in a magnetic field [J]. Nature, 1991, 349: 770−772.

[7] PENG Xiao-ling, ZHANG Ao, LI Jing, YU Shi-yan, CHANG Jia-song, GE Ming-hui, YANG Yan-ting, XU Jing-cai, HONG Bo, JIN Ding-feng, JIN Hong-xiao, WANG Xin-qing, GE Hong-liang, FANG Jian-fei. Design and fabrication of Fe−Si−Al soft magnetic composites by controlling orientation of particles in a magnetic field: Anisotropy of structures, electrical and magnetic properties [J]. Journal of Materials Science, 2019, 54(11): 8719−8726.

[8] SHUAI San-san, WEN Shuo-kai, GUO Rui, WANG Jiang, REN Zhong-ming. Research progress on solidification and nucleation of metals under magnetic fields [J]. Foundry Technology, 2022, 43: 699−712.

[9] LUO Lei, XIA Hong-ying, LUO Liang-shun, SU Yan-qing, CAI Chao-jun, WANG Liang, GUO Jing-jie, FU Heng-zhi. Eliminating shrinkage defects and improving mechanical performance of large thin-walled ZL205A alloy castings by coupling travelling magnetic fields with sequential solidification [J]. Transactions of Nonferrous Metals Society of China, 2021, 31(4): 865−877.

[10] MILYUTIN V A, GERVASYEVA I V. Thermally activated transformations in alloys with different type of magnetic ordering under high magnetic field [J]. Journal of Magnetism and Magnetic Materials, 2019, 492: 165654.

[11] DONG Shu-lin, LIU Tie, DONG Meng, GUO Xiao-yu, YUAN Shuang, WANG Qiang. Enhanced magnetostriction of Tb−Dy−Fe via simultaneous ⟨111⟩ crystallographic orientation and morphological alignment induced by directional solidification in high magnetic fields [J]. Applied Physics Letters, 2020, 116(5): 053903.

[12] LOU Chang-sheng, LIU Tie, DONG Meng, WU Chun, SHAO Jian-guo, WANG Qiang. Magnetic anisotropy induced by crystallographic orientation and morphological alignment in directionally-solidified eutectic Mn−Sb alloy [J]. Journal of Magnetism and Magnetic Materials, 2017, 424: 365−370.

[13] BRAITHWAITE D, BEAUGNON E, TOURNIER R. Magnetically controlled convection in a paramagnetic fluid [J]. Nature, 1991, 354(6349): 134−136.

[14] LI Xi, FAUTRELLE Y, GAGNOUD A, DU Da-fan, WANG Jiang, REN Zhong-ming, NGUYEN-THI H, MANGELINCK-NOEL N. Effect of a weak transverse magnetic field on solidification structure during directional solidification [J]. Acta Materialia, 2014, 64(2): 367−381.

[15] XIAO Yu-bao, LIU Tie, TONG Yu-xin, DONG Meng, LI Jin-shan, WANG Jun, WANG Qiang. Microstructure evolution of peritectic Al−18at.%Ni alloy directionally solidified in high magnetic fields [J]. Journal of Materials Science & Technology, 2021, 76: 51−59.

[16] REN Zhong-ming, WANG Jiang, ZHAO Rui-xin. Orientation and alignment during materials processing under

high magnetic fields [J]. Chinese Physics B, 2019, 28(4): 048301.

[17] ASAI S, SASSA K S, TAHASHI M. Crystal orientation of non-magnetic materials by imposition of a high magnetic field [J]. Science and Technology of Advanced Materials, 2003, 4(5): 455−460.

[18] LIU Chun-mei, ZHONG Yun-bo, SHEN Zhe, DONG Li-cheng, ZHENG Tian-xiang, REN Wei-li, LEI Zuo-sheng, REN Zhong-ming. Effect of a transverse weak magnetic field on the texture evolution and magnetic property of Fe−1.0wt.%Si alloy during bulk solidification [J]. Materials Research Express, 2019, 6: 066105.

[19] LIU Chun-mei, ZHONG Yun-bo, SHEN Zhe, DONG Li-cheng, ZHENG Tian-xiang, REN Wei-li, LEI Zuo-sheng, REN Zhong-ming. Magnetic field-dependent microstructure evolution and magnetic property of Fe−6.5Si−0.05B alloy during solidification [J]. Journal of Materials Research, 2019, 34(24): 4076−4084.

[20] DONG Meng, LIU Tie, GUO Xiao-yu, DONG Shu-lin, LI Lei, WANG Jun, LI Jin-shan, ZHAO Li-jia, WANG Qiang. Crystal orientation induced by high magnetic fields during peritectic reaction of alloys [J]. Materials Characterization, 2022, 183: 111608.

[21] LI Xi, FAUTRELLE Y, REN Zhong-ming, ZHANG Yu-dong, ESLING C. Effect of a high magnetic field on the Al−Al_3Ni fiber eutectic during directional solidification [J]. Acta Materialia, 2010, 58: 2430−2441.

[22] MULLIS A M, JEGEDE O E, BIGG T D, COCHRANE R F. Dynamics of core−shell particle formation in drop-tube processed metastable monotectic alloys [J]. Acta Materialia, 2020, 188: 591−598.

[23] SHOJI E, ISOGAI S, SUZUKI R, KUBO M, TSUKADA T, KAI T, SHINOHARA T, MATSUMOTO Y, FUKUYAMA H. Neutron computed tomography of phase separation structures in solidified CuCo alloys and investigation of relationship between the structures and melt convection during solidification [J]. Scripta Materialia, 2020, 175: 29−32.

[24] ZHAO Dan-dan, GAO Jian-rong. Liquid phase separation in undercooled Cu−Co alloys under the influence of static magnetic fields [J]. Philosophical Transactions of the Royal Society A, 2019, 377(2143): 20180207.

[25] SUGIOKA K I, INOUE T, KITAHARA T, KUROSAWA R, KUBO M, TSUKADA T, UCHIKOSHI M, FUKUYAMA H. Study on the effect of melt convection on phase separation structures in undercooled CuCo alloys using an electromagnetic levitator superimposed with a static magnetic field [J]. Metallurgical and Materials Transactions B, 2014, 45(4): 1439−1445.

[26] WEI Chen, WANG Jun, HE Yi-xuan, LI Jin-shan, BEAUGNON E. Influence of high magnetic field on the liquid−liquid phase separation behavior of an undercooled Cu−Co immiscible alloy [J]. Journal of Alloys and Compounds, 2020, 842: 155502.

[27] WANG Jun, HE Yi-xuan, LI Jin-shan, HU Rui, KOU Hong-chao, BEAUGNON E. Experimental platform for solidification and in-situ magnetization measurement of undercooled melt under strong magnetic field [J]. Review of Scientific Instruments, 2015, 86(2): 025102.

[28] WEI Chen, WANG Jun, HE Yi-xuan, YAN Yu-jie, GAO Jiang-lin, LI Jin-shan, BEAUGNON E. Liquid−liquid phase separation in immiscible Cu−Co alloy [J]. Materials Letters, 2020, 268: 127585.

[29] MASAHASHI N, MATSUO M, WATANABE K. Development of preferred orientation in annealing of Fe−3.25%Si in a high magnetic field [J]. Journal of Materials Research, 1998, 13: 457−461.

[30] ZUO Xiao-wei, WANG En-gang, HAN Huan, ZHANG Lin, HE Ji-cheng. Magnetic properties of Fe−49%Sn monotectic alloys solidified under a high magnetic field [J]. Journal of Alloys and Compounds, 2010, 492(1/2): 621−624.

[31] REHMAN S U, WEI Chen, HUANG Qing-fang, JIANG Qing-zheng, HAQ A U, WANG Jun, ZHONG Zhen-chen. Tailoring the microstructure, magnetic properties and interaction mechanisms of Alnico-Ta alloys by magnetic field treatment [J]. Journal of Alloys and Compounds, 2021, 857: 157586.

[32] NIKITIN S A, IVANOVA T I, ZVONOV A I, KOSHKID'KO Y S, ĆWIK J, ROGACKI K. Magnetization, magnetic anisotropy and magnetocaloric effect of the Tb0.2Gd0.8 single crystal in high magnetic fields up to 14 T in region of a phase transition [J]. Acta Materialia, 2018, 161: 331−337.

[33] LI Lei, ZHANG Rui-xue, BAN Chun-yan, ZHANG Hai-tao, LIU Tie, ZHANG Hui, WANG Xiang-jie, ESLING C, CUI Jian-zhong. Growth behavior of Zn-rich phase in Zn−Mg alloy under a high magnetic field [J]. Materials Characterization, 2019, 151: 191−202.

[34] MIKELSON A E, KARKLIN Y K. Control of crystallization processes by means of magnetic fields [J]. Journal of Crystal Growth, 1981, 52: 524−529.

[35] MICHAUD B, BEAUGNON E, SULPICE A, TOURNIER R, CLAVERIE J. Experimental study of the magnetic orientation of ceramic fibers [J]. Materials Transactions, 2000, 41: 962−965.

[36] LI Xi, FAUTRELLE Y, GAGNOUD A, MOREAU R, DU Da-fan, REN Zhong-ming, LU Xiong-gang. EBSD study on the effect of a strong axial magnetic field on the microstructure and crystallography of Al−Ni alloys during solidification [J]. Metallurgical and Materials Transactions A, 2016, 47(3): 1180−1197.

[37] SUN Zhi, GUO Mu-xing, VLEUGELS J, VAN DER BIEST O, BLANPAIN B. Strong static magnetic field processing of metallic materials: A review [J]. Current Opinion in Solid State and Materials Science, 2012, 16(5): 254−267.

[38] SUGIYAMA T, TAHASHI M, SASSA K, ASAI S. The control of crystal orientation in non-magnetic metals by imposition of a high magnetic field [J]. ISIJ International, 2003, 43(6): 855−861.

[39] YAMAGUCHI M, TANIMOTO Y. Magneto-science: Magnetic field effects on materials: Fundamentals and applications [M]. Tokyo: Kodansha, 2006.

[40] COEY J M D. Magnetism and magnetic materials: Magnetostatics [M]. New York: Cambridge University Press, 2010.

强磁场下 Cu−Co 难混溶合金凝固过程中晶体取向和性能的调控

魏 晨[1]，李金山[1]，闫育洁[1]，贺一轩[1]，Eric BEAUGNON[2]，王 军[1]

1. 西北工业大学 凝固技术国家重点实验室，西安 710072；
2. Univ. Grenoble Alpes, INSA Toulouse, Univ. Toulouse Paul Sabatier, EMFL, CNRS, LNCMI, 38000 Grenoble, France

摘 要：对 $Cu_{50}Co_{50}$ 合金在不同磁场强度下进行非平衡凝固实验，研究富钴相的取向、显微组织演化和磁性能。结果表明，凝固后相分离的棒状富钴相可以实现排列形态，在 5 T 强磁场下富钴相的晶体取向为⟨111⟩平行磁场方向。然而，发生二次液−液相分离的富铜相的取向没有受到 HMF 的显著影响。在 0 T 磁场下凝固的合金表现出近磁各向同性行为，而在 5 T 磁场下凝固的合金则表现出磁各向异性行为。合金的饱和磁化强度略有增加，矫顽力相应降低，这与富钴晶体的取向演化行为密切相关。

关键词：强磁场；显微组织演化；铜钴合金；相分离；磁性能

(Edited by Xiang-qun LI)